Evolution of stress fields and phase content in corroded zirconium cladding materials

Evolution of stress fields and phase content in corroded zirconium cladding materials

Kok Boon Chong, Michael E. Fitzpatrick

PII: S0257-8972(17)30551-0
DOI: doi: 10.1016/j.surfcoat.2017.05.072
Reference: SCT 22391

To appear in: *Surface & Coatings Technology*

Received date: 11 November 2016
Revised date: 19 May 2017
Accepted date: 24 May 2017

Please cite this article as: Kok Boon Chong, Michael E. Fitzpatrick , Evolution of stress fields and phase content in corroded zirconium cladding materials, *Surface & Coatings Technology* (2017), doi: 10.1016/j.surfcoat.2017.05.072

Evolution of Stress Fields and Phase Content in Corroded Zirconium Cladding Materials

Kok Boon Chong[a,c*], Michael E. Fitzpatrick[a,b†]

[a]Department of Engineering & Innovation, The Open University, Walton Hall, Milton Keynes, MK7 6AA, UK.
[b]Centre For Manufacturing & Materials Engineering, Coventry University, Engineering & Computing Building, Priory Street, Coventry CV1 5FB, UK.
[c]Jeffrey Sachs Center on Sustainable Development, Sunway University, No 5, Jalan University, Bandar Sunway, 47500 Selangor, Malaysia.

In this study, the evolution of stress fields and structural phase composition have been studied using Raman spectroscopy pre- and post-transition in the oxide layer of re-crystallised ZIRLO and recrystallised zircaloy-4 (Zr-4) after corrosion exposure in a static autoclave. The structural phase composition analysis showed that the proportion of the tetragonal zirconia phase on the surface decreased with increasing corrosion time. High compressive stresses were found in the thin oxide, increasing with corrosion time, reaching a maximum in the transition period and decreasing slightly after that. The results show the relationship between the crystallographic phase and the residual stresses developed in the oxide.

Keywords: Zr Corrosion, Stress Fields, Phase Content, Raman Spectroscopy.

1 Introduction

Zirconium (Zr) alloys are widely used in nuclear reactor applications such as fuel cladding / channel materials, owing to their low neutron absorption cross-section, high mechanical strength and good corrosion resistance. Corrosion in zirconium alloys is a complicated electrochemical process which is influenced by several factors, including the properties of the metal/oxide interface, water chemistry, pressure, irradiation, and time. Although many reported works[1-9] have studied numerous factors affecting the corrosion processes, and considerable understanding of the corrosion mechanisms have been secured, there are many effects that are still not fully understood: in particular, the relationships between the residual stresses that are generated between the oxide film and the substrate, the structural phase content, and the kinetics of corrosion. Better understanding can lead to the development of alloys

* kokboonc@sunway.eduy.my
† ab6856@coventry.ac.uk

with delayed transition in the oxide corrosion, and hence to improved fuel burn-up and improved efficiency of nuclear reactors.

Several researchers have noted that the oxide comprises a metastable tetragonal phase and an energetically stable monoclinic phase of ZrO_2[7-13]. The tetragonal phase develops locally when oxidation occurs; it has a smaller grain size and is believed to be stabilised by the high compressive stress in the oxide layer[5-11,14,20]. As the oxidation progresses, the formation of new oxide near the metal/oxide interface, moving inward to the alloy substrate, triggers a phase transformation in the oxide film resulting from a complex process. Most of the reported literature indicates a relationship between the amount of tetragonal phase and the corrosion resistance in zirconium alloys[2,4-12], which motivated us to carried out a systematic study from the very beginning to a late stage in zirconium corrosion.

In the present paper, we present results obtained from Raman spectroscopy from oxide layers grown on corroded ZIRLO and Zr-4 specimens. Table 1 tabulates the principal chemical composition for these two alloys. We present measurements of the residual stresses and structural phase fraction in the oxides grown on these two alloys to investigate the mechanisms of corrosion and phase transformation in the oxide.

2 Experimental details

Two batches of materials were characterised in the present study:

(I) Long-term-autoclave recrystallised sheet ZIRLO samples provided by Westinghouse, that had been steam tested at 415°C for 660 days by Sandvik, Sweden;

(II) Short-term-autoclave recrystallised ZIRLO and Zr-4 sheet, which were corrosion tested at EDF R&D in Moret-sur-Loing, France, at 360°C and with a saturation pressure of around 18 MPa in a static autoclave using primary water chemistry (pure H_2O with additions of 2 ppm LiOH and 1000 ppm boric acid).

The details of these materials have been reported elsewhere [3, 14].

Figure 1 depicts the corrosion kinetics of these samples, and figure 2 shows a cross-section of a typical oxide/metal interface, with the characteristic layered structure of the oxide. The main aim was to study the early stage of corrosion, before, during, and after the first transition. Generally, samples that were in the process of going, or had

just gone, through transition displayed a patchy oxide of lighter (region has already gone through transition) and darker regions (region has not yet gone through transition). For Zr-4, the first patchy samples were observed after 180 days while ZIRLO displayed a patchy oxide after 140 days.

The Raman measurements were carried out using an optical-fibre-probe, energy-dispersive Raman spectrometer. An excitation laser with 405 nm wavelength and 150 mW and 15 mW were employed in this study for long- and short-term autoclave specimens respectively. The reason for choosing a slightly lower intensity of the laser is to avoid local heating occurring in the sample which might cause local phase transformation. The laser beam had a diameter of (5.0±0.2) μm in the characterization of the long-term autoclave specimens; a diameter of (0.8±0.1) μm was used for the short-term autoclave specimens. The penetration depth of the spectroscopy in this study is less than 100 nm. The penetration depth is affected by several factors: chemical composition, secondary phase particles, cracks/voids and the high refractive index of zirconium (n ~ 2.2). About 30% of the laser beam was reflected from the surface of the specimen. The specimen was placed directly on the fully automated stage of an optical microscope whose objective lens enables the laser beam to be focused on a particular position. This allows the Raman spectroscopy to be carried out with accurate positioning and allows automated spatial mapping. The spectral range extended from 200 to 850 cm^{-1}. Microcomputer control enabled an averaged Raman spectrum to be obtained in acquisition time of 15 minutes, and corrected for background noise based on a spectrum obtained without illumination. A statistical average of 50 spectra for each measurement was carried out in order to account for any inhomogeneity in a particular location caused by defects etc.

The residual stress was calculated using a simple relationship given by[15,16]

$$\mathrm{RamanShift} = \Pi.\sigma \tag{1}$$

where Π is the piezo-spectroscopy constant; and σ is stress. The piezo-spectroscopy constant was obtained by carefully loading a monoclinic laboratory-prepared zirconia bar similar to the calibration materials use by previous works[8,11,26] in a jig with uniform uniaxial compression, giving $\Pi = -1.69 \mathrm{cm}^{-1}/\mathrm{GPa}$ for the 381_m band. The strongest 460_m band was found to shift very little under uniaxial compression: thus the piezo-spectroscopy constant was calibrated using the 381_m band. The peak positions within each spectrum were then obtained by a fitting procedure using commercial

software (GRAMS, Thermo Electron Corp, Philadelphia), assuming mixed Gaussian and Lorentzian profiles; however, this peak fitting method induced some bias in the peak position owing to the peaks' asymmetry. The peak fits have an accuracy of ± 0.05 cm^{-1}, which is equivalent to an accuracy of ±28 MPa in the calculated stresses. Comparison of the measured Raman bands from the corroded specimens with the bands measured from the powder ZrO_2 provides the Raman band shift caused by the stresses generated during the corrosion processes. The measured stresses were computed by substituting the Raman band shift obtained as described above using Eq. (1). As the laser beam spot is relatively large relative to the grain size, thus the resulted Raman spectra were averaged values from the measured grains under each beam spot. Therefore the measured stresses in this work are the grain-averaged stresses measured in-plane where the Raman spectra have been collected.

The crystallographic phase content was determined from the respective volume fractions of the two phases of tetragonal and monoclinic zirconia[17]. Using the ratio of the intensity of the tetragonal peak at 445 cm^{-1} to its surrounding monoclinic peaks at 382 and 475 cm^{-1}:

$$\%T_{ZrO_2} = \frac{I(445_T)}{[I(382_m)+I(445_T)+I(475_m)]}\times 100\% \quad (2)$$

As the phase fraction calculation was originally established for the 260_T band[17] instead of the 445_T band, thus results of the phase fraction calculated with the modified version in Eq. (2) are likely biased as the main tetragonal band is 260_T. Therefore the calculated phase fraction was a rough estimation, as we did refer to adjacent monoclinic peaks.

3 Results

3.1 Long term autoclave specimen (415˚C / steam, 660 days)

SEM analysis indicated that the long-term autoclave ZIRLO specimen has an oxide layer of about 80 μm thickness (figure 2), and the metal/oxide interface has a typical undulating morphology. The oxide layer is full of periodic lateral cracks, but interestingly there are some regions where the oxide, above the apexes of the metal/oxide interface undulations, are crack-free, which has been attributed to the formation of columnar ZrO_2 grains with a preferred orientation [11-14].

The Raman spectra obtained from the cross section of the specimen are shown in Figure 3(b). Near to the interface, the Raman spectra included a tetragonal peak at 266.9 cm^{-1}, but this tetragonal peak disappears when moving to a distance of about 7.5 μm (beam-centre position) away from the interface. Owing to the increasing incidence of lateral cracks in this thick oxide with distance away from the metal/oxide interface, the Raman spectra became too noisy, as the signal was scattered too much where the beam falls into the cracks. Therefore, the Raman characterization was only able to be carried out in the oxide up to 22.5 μm (beam-centre position) away from the metal/oxide interface in this sample, and the Raman spectrum shown in Figure 3(b) for a distance of 22.5 μm clearly shows only monoclinic peaks and no tetragonal peak. The Raman spectra for distances of 7.5-17.5 μm are similar to the Raman spectrum at 22.5 μm, and thus only the inner and the outer Raman spectra are presented here for clarity. A high compressive stress of about –600 MPa was found in the oxide near the metal/oxide interface as shown in Figure 3(a), which reduces monotonically with distance through the oxide. The compressive stress in the oxide decreases to –40 MPa at a distance of 22.5 μm away from interface. A large beam spot (5 μm diameter) was employed in this characterization, resulting in an averaging of the stress over the equivalent area. The results are in good agreement with measurements obtained using synchrotron X-ray diffraction, that show a steep stress gradient close to the metal/oxide interface, with a shallower gradient after a few microns away from the interface[14]. The stress profile in the metal substrate shows a similar trend of decreasing with distance away from interface: the tensile stress in the metal is about 55 MPa close to interface and has almost vanished at a distance of 22.5 μm from the interface. The tensile stresses in the metal substrate were small but were enough to provide force balance to the large compressive stress in the oxide film, given that the lower stresses acted over the much thicker metal substrate. However, we need to stress that the weak signal collected from the metallic Zr substrate will include a contribution from both the ultra-thin protecting oxide (2-3 nm) layer and the metallic Zr substrate, which might slightly affect the absolute magnitude of the estimated tensile stresses but not the trends of evolution for the estimated stress fields.

3.2 Short term autoclave specimen (360˚C /18MPa/primary water)

Figure 1 illustrates the corrosion kinetics for sheet ZIRLO and Zr-4. The oxidation kinetics for both alloys follow a parabolic/cubic type progression pre-transition, and the ZIRLO has a slightly higher corrosion rate than the Zr-4. In the pre-transition stage, both alloys have corrosion kinetics with exponent *n* about 0.35 to 0.4 when applying the exponential growth function seen in previous work [3,14]. The data suggests that the ZIRLO has gone through transition at about 114 days and the Zr-4 will go through transition at about 160 days as indicated in Figure 1. The origin of the transition is still uncertain, although in general it is believed to be linked to a martensitic-type phase transformation from tetragonal to monoclinic, with an associated 5% volume increase which causes the macroscopic cracks[8,18,19].

Raman spectroscopy analysis was employed to characterize the evolution of the crystallographic phase fraction and the residual stress profile on the top surface of the oxide grown on the short-term autoclave specimens. The Raman spectra obtained from the top surface of the oxide grown on ZIRLO corroded from 54 days (pre-transition) to 180 days (post-transition) are showb in Figure 4. There are only two tetragonal peaks, with wavenumbers of 237_T and 445_T, observed in the Raman spectra for the early stage (54-74 days) of corrosion; but the third tetragonal peak, with a wavenumber of 641_T is observed with further corrosion (94-114 days) approaching the transition stage. An interesting observation is that the main tetragonal band 260_T reported in the literature [8,11,26] was only observed in the Raman spectrum of the long-term autoclaved (415˚C / steam) specimen but not for the short-term autoclaved (360˚C /18MPa/primary water) specimens. The reason for this absence still remains unclear: contributing factors could include the water chemistry, environment, temperature, exposure time, stage of corrosion, as well as the alloy composition of the Zr alloys.

Another interesting observation is that the 237_T band has a broader peak shape. This motivated us to perform a theoretical First-principles calculation of Raman bands via using the open source suite ABINIT package[27]. In the theoretical calculation, we have utilising the pseudo-potential and a plane-wave method within the Density Functional Theory. With allowing the crystallography symmetry to vary, our simulation results reasonably matched with the reported works[24-25]. The measured 237_T band is believed to be a slightly-distorted tetragonal (pseudo-tetragonal) phase with lattice **a**=**b**=**c** but with angle α = 103.79˚ as compared to the $230_{\text{pseudo-T}}$ band in

Table 2. The monoclinic band 294_m was attributed to a shifted monoclinic 304_m band in the reference powder, rather than a very large shift from the tetragonal 260_T in powder. Shortly after the transition (134 days), only the tetragonal peak at 445_T, with a very weak intensity, can be resolved; and no tetragonal peak is observed in the Raman spectrum obtained on the top surface of the oxide layer after corrosion for about 180 days. The intensity for the 237_T and 445_T tetragonal bands increases with oxidation time up to 94 days, but decreases with further oxidation time. It is clearly seen that the tetragonal peaks are better defined in the earlier stage of corrosion pre-transition, and then become broader post-transition, indicating the evolution of the tetragonal phase fraction and the residual stress with increasing corrosion. The Raman spectra obtained from the top surface of the oxide layer obtained from Zr-4 have a similar trend, but the tetragonal peak at 445_T can still be observed after 180 days. However, one should bear in mind that the transition stage for Zr-4 is later, at about 160 days.

For brevity, we do not show the Raman spectra for Zr-4 here, but the analyses are depicted in Figures 5 and 6. According to space-group theory, ideally one should be able to observe six tetragonal peaks and 12 monoclinic peaks[16,17] over the whole range of wavenumbers, but because of the limitation of sensitivity in the equipment, the three tetragonal peaks and eight monoclinic peaks observed in this study are acceptable considering the range of wavenumber attainable.

Figure 5 depicts the tetragonal phase fraction and stress profiles obtained from the top surface of the oxide layer grown on both ZIRLO and Zr-4 alloys for different corrosion stages. It shows that the tetragonal phase fraction at the top surface is about 15% after 54 days for ZIRLO and 17.5% after 80 days for Zr-4. For both alloys, the tetragonal phase fraction at the top surface of the oxide layer decreased at about the same rate as transition approached, but relatively there is a higher tetragonal phase fraction on the top surface found in Zr-4 than ZIRLO. The results are reconfirmed the reported trends in the residual stresses and tetragonal phase reported by Polatidis[28], Panicuad[29] and Gurain[30]. The origin for the difference in the absolute tetragonal phase fraction is not understood yet given that both Zr alloys have similar alloying except Nb and Cr.

The measured stress on the top surface for ZIRLO corroded for 54 days is about –0.45 GPa, which increases approaching transition (114 days) to about –0.9 GPa on the top surface. After transition, stress relaxation has occurred with

compression of about –0.7 GPa at 134 days, and subsequently the stress becomes slightly more compressive with further corrosion. It must be emphasised here that all the stress profiles reported are for the monoclinic phase, as the tetragonal phase is not detected for all the specimens and furthermore the piezo-spectroscopy constant is based on the shift of the monoclinic peak. Furthermore, the tetragonal phase is not detectable on the top surface of the oxide layer in the later stages after transition for the ZIRLO specimens.

For the Zr-4 specimen, the measured stress on the top surface of the oxide layer is a compressive stress of about –0.89 GPa at 80 days of corrosion, increasing to –1.7 GPa at transition (160 days of corrosion), and then the stress relaxation is much smaller than in ZIRLO, to a compressive stress of –1.43 GPa for the monoclinic phase in the specimen corroded for 180 days. In both cases, the compressive stress seems to have its maximum value at the transition stage, and relaxes to a lower magnitude with further corrosion. These results agree with the trends of changes in stress profiles obtained from synchrotron X-ray diffraction which was reported in previous work[9,14].

As Raman spectroscopy is a surface technique, the analysis only examines the outer layer of the oxide which formed at the very beginning of the corrosion process. As the corrosion advances, the metal/oxide interface moves inward to the substrate, and therefore some Raman spectroscopy was carried out on the cross-section of the specimen as for the 180 days autoclaved specimen. Figure 6 shows the stress profile obtained from these Raman experiments for both alloys corroded for about 180 days. The compressive stresses for the monoclinic phase in the oxide layer are larger in Zr-4 compared to ZIRLO for a given distance in the oxide away from the metal/oxide interface. However, the ZIRLO has a thicker oxide layer compared to the Zr-4 as shown in Figure 1. At a distance very close (about 0.43 μm) to the metal/oxide interface, the ZIRLO has a compressive stress of –1.39 GPa, and the Zr-4 has –2.36 GPa. The stress profile decreases towards the outer layer of the oxide in both cases, with a reduction of about 0.64 GPa and 0.96 GPa comparing the stress in the oxide close to the interface and on the top surface of the oxide for ZIRLO and Zr-4 respectively. Although the absolute reduction of stress is larger in the Zr-4 than the ZIRLO, the relative reduction of stress is about the same comparing the top surface and the oxide near the interface.

4. Discussion

The main aim of the present study was to investigate the mechanism of zirconium corrosion, linking the structural phase fraction and residual stress fields with the corrosion kinetics.

The stress results for a thick oxide (from the long-term autoclave samples) indicate that stress relaxation is taking place in the oxide as the metal/oxide interface moves inwards. Although some researchers have demonstrated that the large compressive stress in the oxide layer can result in creep of the entire corrosion film[18,19,26,28,29], the large gradient of the stress relaxation in the oxide suggests that additional mechanisms could be responsible for this stress relaxation. The stress relaxation process could be induced by the development of cracks and porosity in the oxide layers, and subsequent delamination of the oxide layers which degrades the protective properties of the oxide[22,26,30] and may lead to the increase in corrosion rate post-transition.

It is important to remember that the outer layer of oxide in the short-term autoclave specimens had already formed before the alloys were inserted into the autoclave, and this oxide has slightly higher tetragonal phase content before the corrosion process. The tetragonal phase fraction on the top surface of the oxide in both specimens decreased with corrosion time, but it is interesting to note that a third tetragonal peak, 641_T occurred when approaching transition. This is suggesting that the transition could be an order-disorder-type transformation, as the metastable tetragonal peak at the autoclave temperature has to suddenly transform to monoclinic after the transition. In addition, the present of Nb^{5+} has been suggested as contributing to the destabilisation of the tetragonal form[23], which is consistent with the Raman results that the tetragonal phase fraction is higher in the Zr-4 specimen than ZIRLO.

The results indicate that the compressive stress on the top surface of the oxide increases from an early stage of corrosion, and achieves a maximum at the transition stage before partial relaxation of the stress occurs after transition. However, the tetragonal phase fraction on the top surface decreases with corrosion, which could be suggesting that an additional interaction between the newly formed tetragonal phases at the metal/oxide interface and the previously-formed tetragonal phase at the top surface of the oxide should be taken into consideration, alongside the idea that the large compressive stress stabilises the tetragonal phase content near the metal/oxide interface as proposed by most models[10,21,22,26,28-30]. However, our results have shown

that there is some inconsistency between the tetragonal phase fraction and the magnitude of the compressive stress in the oxide layer. It is essential to note that the tetragonal phase in the oxide is not uniformly distributed and is concentrated at the region near the metal/oxide interface. Thus one should consider the role of the high local stress in stabilising the tetragonal phase[20,28,30], and the steep gradient of macroscopic stress reported in this study. In addition, TEM observations in related work[14] suggested that the equiaxial grains on top surface could be transformed from tetragonal to monoclinic, as the transformation needs higher stress to achieve it[22,31].

Conclusions

Raman spectroscopy has been employed for characterizing a series of autoclave-exposed zirconium alloys, comprising ZIRLO and Zr-4, exposed for increasing times pre- and post- the transition in corrosion kinetics.

1. For the specimens steam tested at 415°C for 660 days, a steep gradient of compressive stress is observed in the oxide, with a high compressive stress that decreases with distance from the metal/oxide interface. A tetragonal phase peak is observed in the oxide, but only at the region close to the metal/oxide interface.
2. For the short-term autoclave specimens exposed to primary water at 360°C for up to 200 days, the tetragonal phase fraction on the top surface of the oxide is higher in the Zr-4 compared to the ZIRLO. This is consistent with a higher compressive oxide residual stress in the Zr-4 than the ZIRLO specimens.
3. For both materials, the compressive stresses in the oxide, measured on the top surface of the sample, increased with corrosion time and oxide thickness, reached a maximum value at the transition, before then relaxing to lower values post-transition. The relaxation of the stress fields correlates with the tetragonal phase fraction, and could be attributed to the release of the stored energy in the oxide scales via crack formation and propagation, creep of the oxide and metal, as well as the tetragonal-to-monoclinic phase transformation of the ZrO_2.

Acknowledgement

The authors would like to thank: the UK EPSRC and the UK Ministry of Defence for funding this research as part of the Materials for Energy call (EP/E036481/1); J. Wei

from the University of Manchester for preparing the autoclave samples; N. Roohpour and A. Ghandour at Queen Mary University of London for access to their Raman facilities; G.-M Riganese of Université Catholique de Louvain and European Theoretical Spectroscopy Facilities for the assistance in the ABINIT simulation; EDF R&D, Westinghouse, Rolls Royce, NNL and SERCO for providing part financial support and valuable materials. MEF is grateful for funding from the Lloyd's Register Foundation, a charitable foundation helping to protect life and property by supporting engineering-related education, public engagement and the application of research. KBC would like to thank The Open University and Sunway University for support in this research.

References

1 B. Cox, *Mechanisms of Zirconium Alloy Corrosion in Nuclear Reactors*, J. Nucl. Mater. **28** (1968) 1-47.

2 S. Kass, *Corrosion of prefilmed zircaloy*, Corrosion, **23** (1967) 374-378.

3 *J*. Wei et al., *Autoclave Study of Zirconium Alloys with and without Hydride Rim*, Corros. Eng. Sci. Technol. **47** (2012) 516-528.

4 E. Anastassakis, B. Papanicolaou and I. M. Ashers, *Lattice dynamics and light scattering in Hafnia and Zirconia*, J. Phys. Chem. Solids **36** (1975) 667-676.

5 A. Yilmazbayhan et al., *Structure of zirconium alloy oxides formed in pure water Studied with synchrotron radiation and optical microscopy: relation to corrosion rate*, J. Nucl. Mater., **324** (2004) 6-22.

6 Y. H. Jeong, K. O. Lee, and H. G. Kim, *Correlation between microstructure and corrosion behavior of Zr–Nb binary alloy*, J. Nucl. Mater., **302** (2002) 9-19.

7 T. Arima et al, *Oxidation kinetics of Zircaloy-2 between 450°C and 600°C in oxidizing atmosphere*, J. Nucl. Mater., **257** (1998) 67-77.

8 J. Godlewski et al., Raman-spectroscopy study of the tetragonal-to-monoclinic transition in zirconium-oxide scales and determination of overall oxygen diffusion by nuclear microanalysis of O-18, 9th Int. Symp. on Zr in the Nucl. Industry, ASTM STP **1132** (1991) 416-436, Kobe, Japan.

9 H. Swan et al., *The Measurement of Stress and phase fraction distributions in pre and post-transition Zircaloy oxides using Nano-beam Synchrotron X-ray Diffraction*, J. Nucl. Mater, **479** (2016), 559-575.

10 C. Roy and B. Burgess, A study of the stresses generated in zirconia films during the oxidation of zirconium alloys, Oxid. Met., **2** (1970) 235-261.

11 J. Godlewski, *How the tetragonal zirconia is stabilized in the oxide scale that is formed on a zirconium alloy corroded at 400°C in steam*, 10th Int. Symp. on Zr in the Nucl. Industry, ASTM Int., **1245** (1994) 663-667, Philadelphia.

12 W. Qin et al, *Effects of local stress on the stability of tetragonal phase in ZrO_2 film*, J. Alloys Comp. **437** (2007) 280-284.

13 A. Yilmazbayhan et al, *Transmission electron microscopy examination of oxide layers formed on Zr alloys*, J. Nucl. Mater. **349** (2006) 265-281.

14 M. Preuss et al, *Studies regarding corrosion mechanism in zirconium alloys*, J. ASTM Int., **8** (2011) 649-681.

15 G. de Portu et al, *Measurement of residual stress distributions in Al2O3/Y-TZP multilayered composite by fluorescence and Raman microprobe piezo-spectroscopy*, Acta Mater., **53** (2005)1511-1520.
16 Q. Ma and D. R. Clarke, *Piezospectroscopic determination of residual stresses in polycrystalline alumina*, J. Am. Ceram. Soc., **77** (1994) 298-302.
17 D. R. Clarke and F. Adar, Measurement of the crystallographically transformed zone produced by fracture in ceramics containing tetragonal zirconia, J. Am. Ceram. Soc., **65** (1982) 284-288.
18 M. Blat-Yrieix et al, Towards a better understanding of dimensional changes in zircaloy-4: what is the impact induced by hydrides and oxide layer, 15th Int. Symp. on Zr in the Nucl. Industry, J. ASTM Int., **5** (2008) 594-609.
19 A. T. Motta et al, *Microstructure and growth mechanism of oxide layers formed in Zr alloys studied with micro beam synchrotron radiation*, J. ASTM Int., **2** (2005)1-26.
20 H. X. Zhang et al., *Crystal structure, corrosion kinetics of new zirconium alloys and residual stress analysis of oxide films*, J. Nucl. Mater., **396** (2010) 65-70.
21 N. Petigny-Putigny, *Comparaison de l'oxydation de deux alliages de zirconium par diffraction des Rayons X in-situ et ex-situ: texture, phase, contrainte*, PhD thesis, University de Bourgogne, 1998.
22 J. Godlewski et al, *A Raman study of the nanocrystallite size effect on the pressure–temperature phase diagram of zirconia grown by zirconium-based alloys oxidation*, J. Nucl. Mater., **300** (2002)118-126.
23 K. Dae-Joon, *Effect of Ta_2O_5, Nb_2O_5, and HfO_2 alloying on the transformability of Y_2O_3-stabilized tetragonal ZrO_2*, J. American. Ceram. Soc., **73** (1990)115-120.
24 V. Milman et al., *Structural, electronic and vibrational properties of tetragonal zirconia under pressure: a Density Functional Theory study*, J. Phys.: Condens. Matter, **21** (2009) 485404.
25 G.-M. Rignanese et al., *First-principles study of dynamical and dielectric properties of tetragonal zirconia*, Phys. Rev. B, **64** (2001) 134301.
26 P. Barberis, T. Merle-Méjean and P. Quintard, *On Raman spectroscopy of zirconium oxide films*, J. Nucl. Mater., **246** (1997) 232-243.
27 http://www.etsf.eu/resources/software/codes
28 E. Polatidis et al., *Residual Stresses and tetragonal phase fraction charaterization of corrosion tested Zircaloy-4 using energy dispersive synchrotron X-ray diffraction*, J. Nucl. Mater., **432** (2013) 102-112.
29 B. Panicaud et al., *On the mechanical effects of a nanocrystallisation treatment for ZrO_2 oxide films growing on a zirconium alloys*, Corros. Sci., **68** (2013) 263-274.
30 M. Guerain et al., *Review of stress fields in zirconium alloys corrosion scales*, Corros Sci., **95** (2015) 11-21.
31 J. Cai et al., *Temperature dependence of Raman scattering in stabilized cubic zirconia*, Phys. Rev. B, **51** (1995) 201-209.

Table 1: Measured chemical composition for zirconium alloys

Alloy	*Zr*	*Fe / wt%*	*Sn / wt%*	*Nb / wt%*	*Cr/ wt%*
ZIRLO	balance	0.1	0.9	0.9	<0.01
Zircaloy-4	balance	0.2	1.2	<0.01	0.1

Table 2: Comparison of the theoretical calculated and experimental measured Raman bands of zirconia. Notation: T=tetragonal phase, M=monoclinic phase

Symmetry	Raman bands / cm^{-1}	
	Calculated	Measured
Pseudo-T (α=103.79˚)	230	237
T	258	266.9
M	469	475
M	608	620
T	639	641

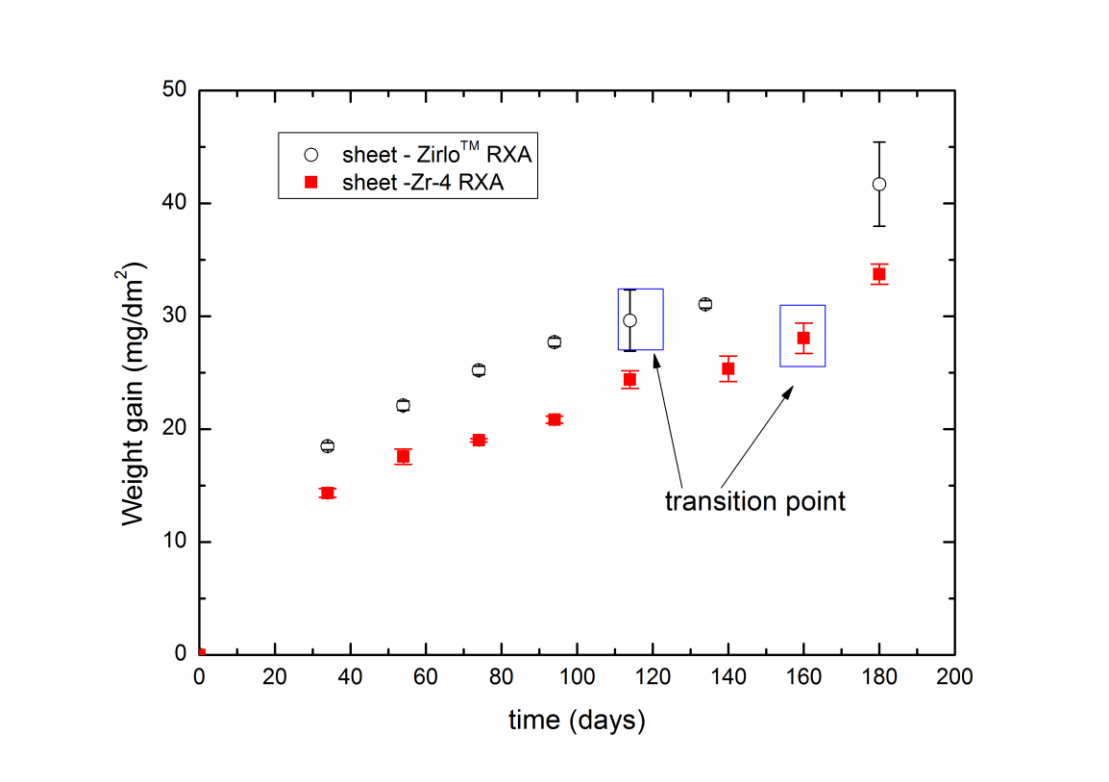

Figure 1. Corrosion kinetics for recrystallised sheet ZIRLO and Zr-4.

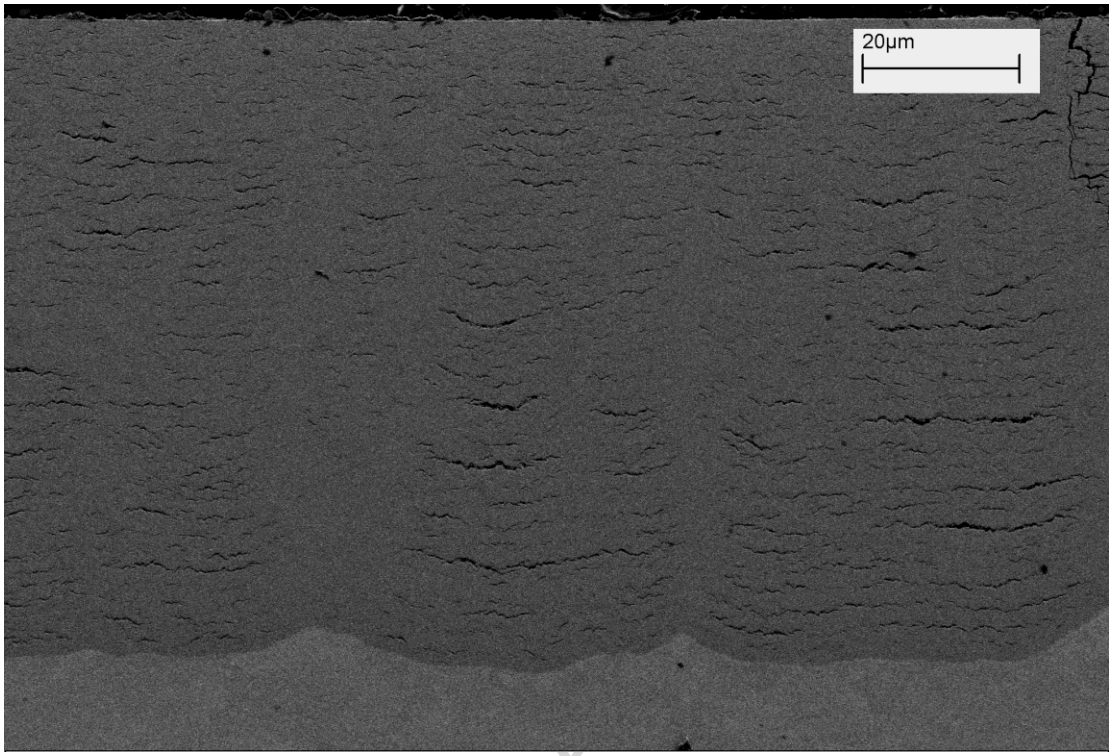

Figure 2. Cross-sectional SEM image of the oxide and metal/oxide interface taken from a long term autoclave ZIRLO specimen.

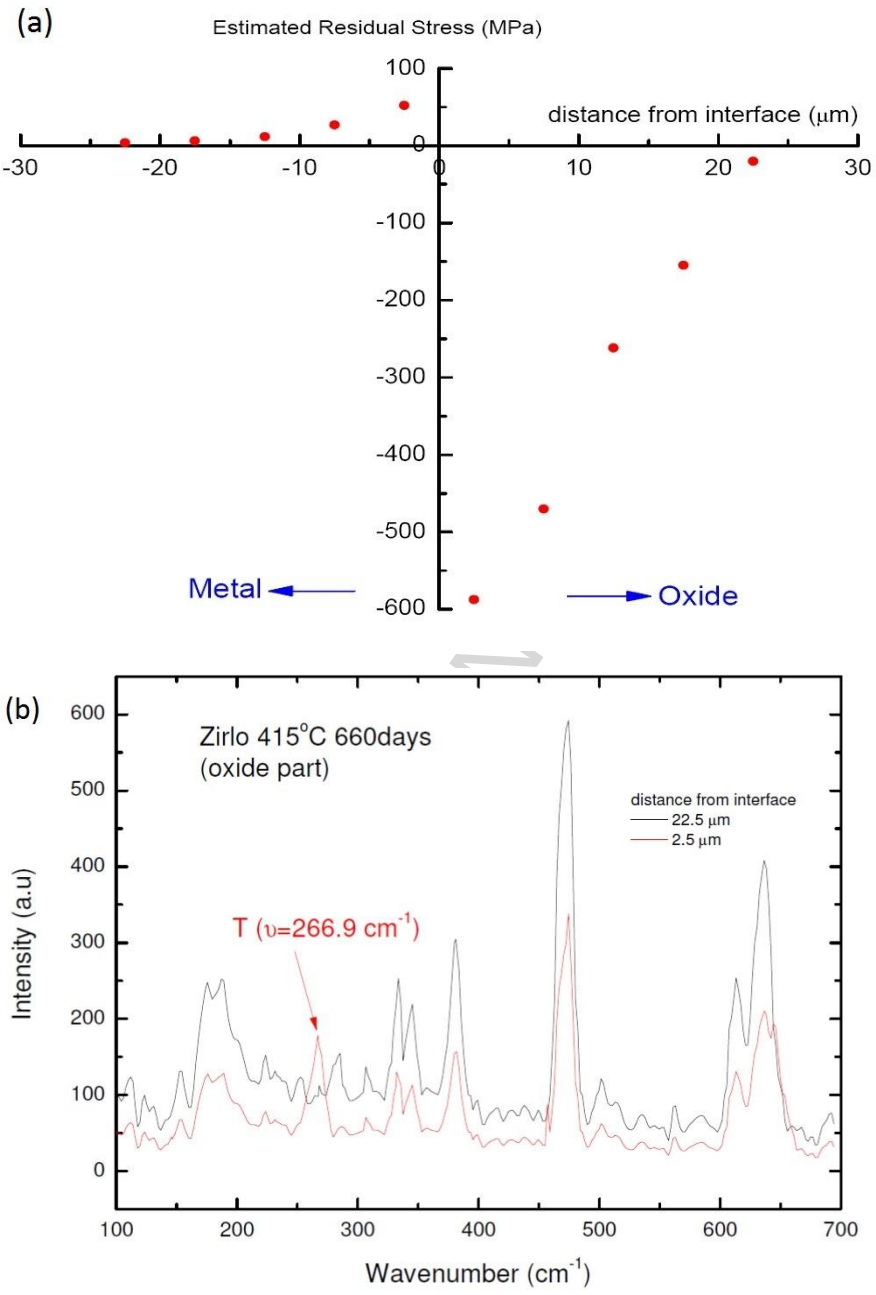

Figure 3. (a) Residual stresses estimated from the Raman peak shift for the long-term autoclave ZIRLO specimen; (b) The Raman spectra at different distances in the oxide layers from the metal/oxide interface.

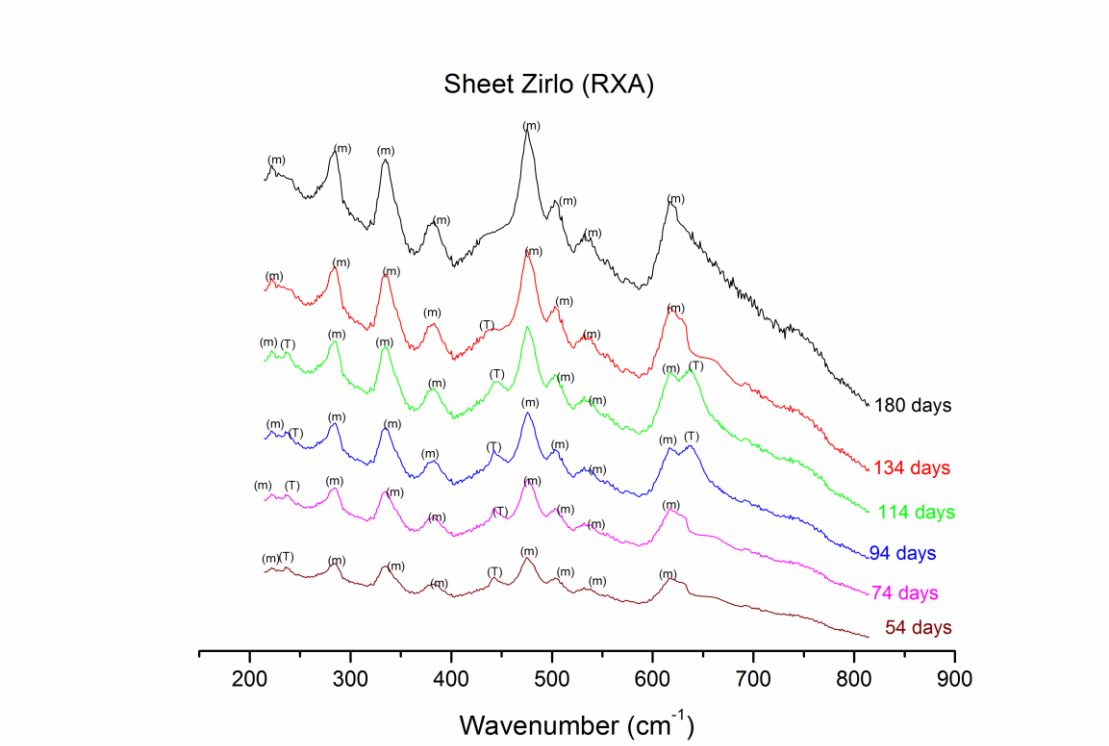

Figure 4. Raman spectra obtained from the surface of the sheet ZIRLO RX at different corrosion stages.

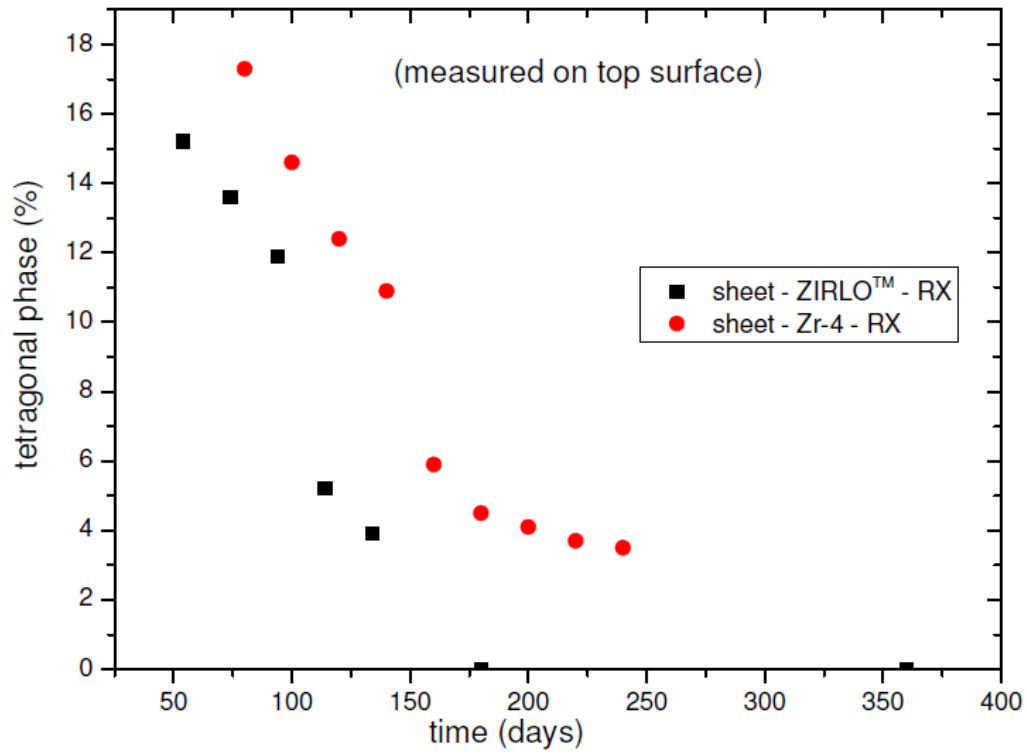

(a)

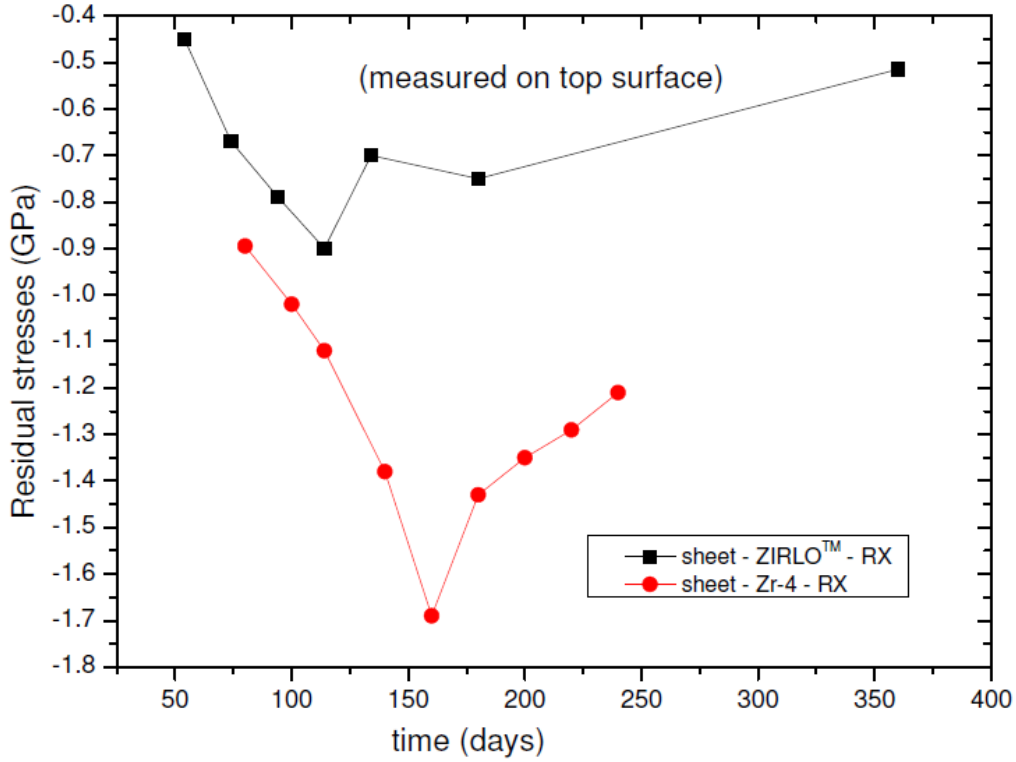

(b)

Fig. 5. Raman characterization on the top surface of the oxide grown on sheet ZIRLO RX and Zr-4 RX specimens: (a) Tetragonal phase fraction, and (b) Measured stress profile.

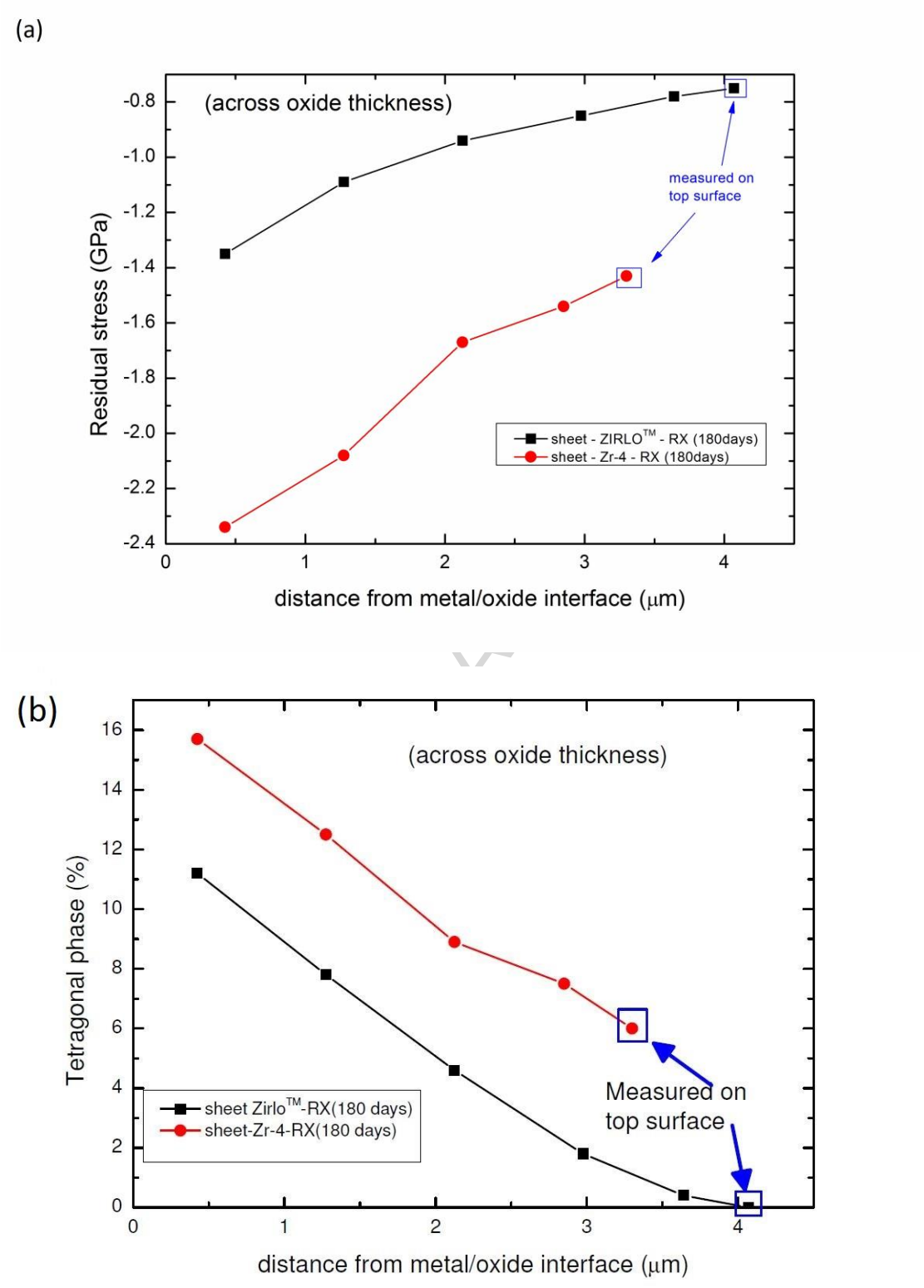

Figure 6. (a) Residual stress profile and (b) tetragonal phase content across the oxide thickness obtained from Raman spectroscopy characterised on a cross-section of the specimens.